Bulletin of Mathematical Biology (2022) 84:116
https://doi.org/10.1007/s11538-022-01070-y

Society for Mathematical Biology

SPECIAL COLLECTION: MODELLING OF BIOLOGICAL SYSTEMS

Understanding the Role of Environmental Transmission on COVID-19 Herd Immunity and Invasion Potential

M.A Masud[1] · Md. Hamidul Islam[2] · Byul Nim Kim[3]

Received: 28 January 2022 / Accepted: 18 August 2022 / Published online: 10 September 2022

Abstract

COVID-19 is caused by the SARS-CoV-2 virus, which is mainly transmitted directly between humans. However, it is observed that this disease can also be transmitted through an indirect route via environmental fomites. The development of appropriate and effective vaccines has allowed us to target and anticipate herd immunity. Understanding of the transmission dynamics and the persistence of the virus on environmental fomites and their resistive role on indirect transmission of the virus is an important scientific and public health challenge because it is essential to consider all possible transmission routes and route specific transmission strength to accurately quantify the herd immunity threshold. In this paper, we present a mathematical model that considers both direct and indirect transmission modes. Our analysis focuses on establishing the disease invasion threshold, investigating its sensitivity to both transmission routes and isolate route-specific transmission rate. Using the tau-leap algorithm, we perform a stochastic model simulation to address the invasion potential of both transmission routes. Our analysis shows that direct transmission has a higher invasion potential than that of the indirect transmission. As a proof of this concept, we fitted our model with early epidemic data from several countries to uniquely estimate the reproduction numbers associated with direct and indirect transmission upon confirming the identifiability of the parameters. As the indirect transmission possess

✉ M.A Masud
masudku03@gmail.com

✉ Byul Nim Kim
air1227@gmail.com

Md. Hamidul Islam
hamidul.islam@ru.ac.bd

1 Natural Product Informatics Research Center, Korea Institute of Science and Technology, Gangneung 25451, South Korea

2 Department of Applied Mathematics, University of Rajshahi, Rajshahi 6205, Bangladesh

3 Institute for Mathematical Convergence, Kyungpook National University, Daegu 41566, South Korea

lower invasion potential than direct transmission, proper estimation and necessary steps toward mitigating it would help reduce vaccination requirement.

Keywords COVID-19 · Vaccination · Indirect transmission · Mathematical modeling · Identifiability

1 Introduction

Coronaviruses are enveloped RNA viruses that use mammals and birds as hosts and have the ability to cause various types of respiratory symptoms (Wardeh et al. 2021; Zhu et al. 2020; Kim and Lee 2020). Two distinguished strains of this virus, namely SARS-CoV and MERS-CoV, have caused several epidemic outbreaks during the last two decades at several places around the world (Zhu et al. 2020). The ubiquity of this virus along with its large genetic diversity and increasing animal–human interactions has amplified the likelihood of the emergence of a coronavirus infection (Huang and Wang 2021). The most recent outbreak of the virus was caused by the novel strain SARS-CoV-2 that led to the recent pandemic of the coronavirus disease 2019 (COVID-19).

In the last two years, significant improvement has been done in understanding the transmission routes and pathways of COVID-19 (Azuma et al. 2020; Rothe et al. 2020; Yu and Yang 2020; Morawska et al. 2020; Pitol and Julian 2021; Castaño et al. 2021). The onset of this disease is usually characterized by symptoms like fever, cough, and sore throat, and in some cases, the severity of the disease leads to shortness of breath. Virus particles discharged through nostrils and mouth during breathing, talking, sneezing, and/or coughing may transmit the disease to other host. COVID-19 patients may spread the disease at least 1–3 days before the onset of their symptoms (Wormser 2020). Furthermore, in many cases (17.8% Mizumoto et al. 2020, 30.8% Nishiura et al. 2020), it has been shown that patients tend to be asymptomatic or simply develop very mild symptoms throughout the entire infectious period. Consequently, patients who are infectious and transmit the disease may go unnoticed, which can be a key driver that undermines any efforts to contain the disease (Bai et al. 2020; Rothe et al. 2020). Another potential driver for transmission could be the prolonged sustenance of the virus on environmental fomites (Vardoulakis et al. 2020; Azuma et al. 2020; Pitol and Julian 2021). In experimental setup, SARS-CoV-2 was found stable on plastic and stainless steel up to 72 h (van Doremalen et al. 2020). On plastic and human skin surfaces, variants of SARS-CoV-2 maintained infectivity for several hours (Hirose et al. 2020, 2022). Gidari et al. reported infectious existence of this virus on plastic and glass for more than 120 h and on stainless steel for more than 72 h (Gidari et al. 2021). Infectious virus was detected even after 7 days on a sample of surgical masks (Chin et al. 2020). SARS-CoV-2 survival for up to 1, 5, and 10 days was reported on fake fur, plastic, and mink fur, respectively (Brown et al. 2021). In artificial saliva, it was found stable for at least 90 min (Smither et al. 2020). Live SARS-CoV-2 RNA was detected on 8.3% of the high-touch surfaces in the public locations during a COVID-19 outbreak in Massachusetts (Harvey et al. 2021). The above literature suggests that an additional key driver for COVID-19 outbreak could be the prolonged sustenance of the virus on

environmental fomites. However, the effectiveness of surface disinfection is highly dependent on the prevalence and the frequency of contact as well as environmental conditions (Gidari et al. 2021; Pottage et al. 2021; Wilson et al. 2021). For instance, approximately 30% of disease transmissions on the Diamond Princess cruise ship were reported to be related to fomite-mediated transmission (Azimi et al. 2021), whereas in China this percentage is reported to be 45–62% (Yang and Wang 2021). In hospital setting, 27% of the environmental surfaces were reported to contain SARS-CoV-2 RNA even though disinfectant were sprayed twice (Kim et al. 2020). Further details pertaining to the deposition, survival, and transmission of the virus can be accessed in Leung (2021), Castaño et al. (2021), Aydogdu et al. (2021), and Gonçalves et al. (2021). The environmental transmission has also been observed to play a critical role in the persistence and inter annual epidemics for other communicable diseases (Vergara-Castaneda et al. 2012; Lopman et al. 2012; McKinney et al. 2006; Breban et al. 2009; Al-Tawfiq and Memish 2016).

Environmental route of transmission has been modeled mathematically for several infectious diseases and was proved to hold important implications for disease control (Eisenberg et al. 2005; Zhao et al. 2012). For instance, environmental transmission modulates the periodicity in avian influenza outbreak (Breban et al. 2009; Rohani et al. 2009; Wang et al. 2012). It is also associated with spatial diffusion of avian influenza (Li et al. 2019). Recently, several mathematical models have been proposed regarding fomite-mediated transmission of COVID-19 (Yang and Wang 2020; Stutt et al. 2020; Yang and Wang 2021; Wijaya et al. 2021; Rwezaura et al. 2021). However, the role of fomite-mediated transmission in crucial public health issues, such as herd immunity, has yet to be substantially explored. Moreover, it would be of interest to evaluate which transmission pathway has a higher invasion potential. In this study, we have classified the transmission routes into two types–direct and indirect. Direct transmission refers to transmission of the infection that comes directly from an infectious to a susceptible individual. In contrast, indirect transmission refers to the deposition of the virus particles by an infectious individual on environmental fomites followed by inoculation of the virus by a susceptible individual who, in turn, becomes infectious.

The remaining part of the paper is structured as follows. We initially present the mathematical model in Sect. 2. We then analyze our model to establish the disease invasion threshold and investigate its sensitivity to both transmission routes in Sect. 3.1. Section 3.2 presents the stochastic simulation wherein we investigate the invasion potential of both transmission routes. Consequently, we fit our model to the early epidemic data obtained from several countries, along with identifiability analysis to quantify route-specific transmission strength (in Sect. 3.3), thereby measuring the vaccination requirement according to initial outbreak data for the acquisition of herd immunity, which is presented in Sect. 3.4. Finally, we discuss and summarize our findings in Sect. 4.

2 Epidemic Model

We divided the human host into four different compartments: susceptible (S), infectious (A), confirmed infected (I), and recovered (R). Furthermore, F represents viruses

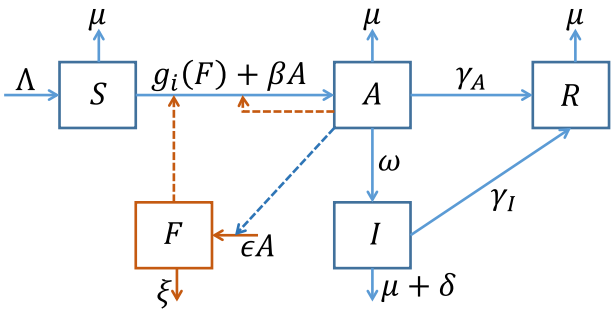

Fig. 1 Flowchart. The squares represent the compartments, solid lines show the flow between the compartments, and dotted line demonstrates the inducing effect of the compartment on the respective flow rate (color figure online)

on environmental carriers or fomites (Fig. 1). Susceptible individuals are the ones who can contract the disease following exposure to the virus. Once a susceptible person is exposed to the virus through direct or indirect contact with an infectious agent, they may either become infectious and express symptoms after a latency period or may not express symptoms albeit transmit the disease. Depending on symptom expression, public health guidelines and the capacity of public health authority to isolate infectious individuals, the infectious individuals may be confirmed/identified as infected, or may remain unnoticed and remain infectious. For simplicity, we assume the confirmed infected individuals no longer transmit the disease. An infected individual may remain infectious throughout his/her whole infectious lifetime and pass through $S \to A \to R$ pathway; or an infected individual may remain infectious in first few days until s/he becomes confirmed at some point of his/her infectious lifetime and pass through $S \to A \to I \to R$ pathway.

When infectious individuals talk loudly, cough, or sneeze, numerous virus particles exit from their respiratory organs and can be deposited on surfaces in the environment, where they can survive for a long time (van Doremalen et al. 2020; Hirose et al. 2020, 2022; Gidari et al. 2021; Chin et al. 2020; Brown et al. 2021; Smither et al. 2020; Harvey et al. 2021) and be carried away by a new host afterward. Virus particles deposited on environmental fomites belong to the F compartment. The rate at which asymptomatic individuals $deposit$ the virus on fomites is ϵ and the viral particles $decay$ naturally at a rate of ξ. We assume that the viral population is large enough to describe the viral population dynamics by the following two processes: $deposit$ and $decay$. In addition, we consider that the probability of infection from a virus picked up from the environmental fomites is a function of daily viral exposure to the environmental fomites. Precisely, we assume that a constant fraction ρ of virions (F) is picked up by each susceptible individual per day and may cause infection with a probability of $g(F_d)$, where $F_d = \rho F$, which reflects the daily pick up rate. We consider the following two types of functional forms for g, which are written as a function of F only for simplicity, as ρ is assumed constant.

Case I $g_1(F) = \pi\rho F = \alpha F$ (Li et al. 2009).
Case II $g_2(F) = 1 - e^{-\pi\rho F} = 1 - e^{-\alpha F}$ (Watanabe et al. 2010; Breban et al. 2009).

where $\alpha = \pi\rho$. Under these assumptions, we obtain the following system of differential equations

$$\begin{aligned}
\frac{\mathrm{d}S(t)}{\mathrm{d}t} &= \Lambda - \beta AS - Sg_i(F) - \mu S \\
\frac{\mathrm{d}A(t)}{\mathrm{d}t} &= \beta AS + Sg_i(F) - (\omega + \gamma_A + \mu)A \\
\frac{\mathrm{d}I(t)}{\mathrm{d}t} &= \omega A - (\gamma_I + \mu + \delta)I \\
\frac{\mathrm{d}R(t)}{\mathrm{d}t} &= \gamma_A A + \gamma_I I - \mu R \\
\frac{\mathrm{d}F(t)}{\mathrm{d}t} &= \epsilon A - \xi F
\end{aligned} \tag{1}$$

3 Results

3.1 Invasion Threshold

The invasion threshold of the disease is determined by the existence and stability of the equilibria.

Proposition 1 *The model has a unique disease-free equilibrium (DFE), $\mathcal{E}_0$. In addition, it has an endemic equilibrium (EE), $\mathcal{E}$ which exists for $R_0 > 1$.*

The basic reproduction number, R_0, is a crucial threshold for characterizing the dynamics of an outbreak. It refers to the average number of secondary infections caused by the introduction of one infectious individual in a completely susceptible population. Here, we designate A and F as the diseased class. The DFE is given by $\mathcal{E}_0 = \left(\frac{\Lambda}{\mu}, 0, 0, 0, 0\right)$.

The next generation matrix at $\mathcal{E}_0$ is given by (Please refer to "Appendix A" for details)

$$K = [K_{i,j}] = \mathfrak{F}\mathfrak{V}^{-1} = \begin{pmatrix} \frac{\Lambda\beta}{\mu k_A} & \frac{\Lambda f_i'(0)}{\mu\xi} \\ \frac{\epsilon}{k_A} & 0 \end{pmatrix} \tag{2}$$

where $k_A = \omega + \gamma_A + \mu$ and $k_I = \gamma_I + \mu + \delta$.

$K_{k,j}$ provides the expected number of secondary infections in class k produced by a single incident in class j. Recent studies (Yang and Wang 2020; Stutt et al. 2020; Yang and Wang 2021; Wijaya et al. 2021), $K_{2,1}$ is considered 0 without considering the environmental fomites (F) as infectious. In this study, we consider both A and F as infectious compartments, and we interpret $K_{1,1}$ as the number of new secondary infectious individuals caused by one infectious individual during his/her entire infectious period, $K_{2,1}$ as the number of virus particles spread by an infectious individual throughout his/her entire infectious period, and $K_{1,2}$ as the number of new infected individual caused by one virus particle in the environment throughout its entire active

period. The spectral radius of K is the basic reproduction number R_0, which is given below

$$R_0 = \rho(K) = \frac{1}{2}\left(\frac{\Lambda\beta}{\mu k_A} + \sqrt{\left(\frac{\Lambda\beta}{\mu k_A}\right)^2 + 4\frac{\Lambda\epsilon\rho\pi}{\mu\xi k_A}}\right)$$

The basic reproduction number can be rearranged and expressed in the following form:

$$R_0 = \frac{1}{2}\left(R_{0H} + \sqrt{R_{0H}^2 + 4R_{0F}}\right)$$

where $R_{0H} = \frac{\Lambda\beta}{\mu k_A}$, $R_{0F} = \frac{\Lambda\rho\epsilon\pi}{\mu\xi k_A}$.

Here, we can highlight the role of direct and indirect transmission. At $\mathcal{E}_0$, an asymptomatic infectious individual transmits disease to $\frac{\Lambda}{\mu}\beta$ individuals per day and the total infectious period is $\frac{1}{k_A}$ days. Therefore, $R_{0H} = \frac{\Lambda}{\mu}\beta\frac{1}{k_A}$ is the expected number of new infections generated from an infected individual throughout his/her entire infectious period. In contrast, infectious individuals deposit virus particles on environmental fomites at a rate of ϵ. The total virus particles deposited in the environment throughout the entire infectious period of a single infected individual is $\frac{\epsilon}{k_A}$. Each virus particle can subsequently infect a person with a probability of α in Case I and $1 - e^{-\alpha} \approx \alpha$ in Case II per day. A virus particle can survive on environmental fomites for an expected duration of $\frac{1}{\xi}$ days. Hence, the expected number of infected individuals caused by a single virus particle in a completely susceptible environment is $\frac{\Lambda}{\mu}\frac{1}{\xi}\alpha$. Therefore, $R_{0F} = \frac{\Lambda\epsilon\pi\rho}{\mu\xi k_A}$ quantifies the expected number of secondary infections as a result of indirect transmission.

A comparison of the role of direct and indirect transmission is portrayed in Fig. 2, which shows that R_0 increases linearly with R_{0H}. In contrast, R_0 increases faster than linear with R_{0F} until $R_0 < 1$. When $R_0 > 1$, the impact of indirect transmission diminishes as R_0 increases, i.e., indirect transmission plays a crucial role if R_0 is near 1.

Theorem 1 *The DFE is locally asymptotically stable for* $R_0 < 1$ *and unstable for* $R_0 > 1$.

Please refer to "Appendix B" for detailed proof. The EE is given by

$$\mathcal{E}_* = (S_*, A_*, I_*, R_*, F_*)$$

where $S_* = \frac{k_A}{\beta + g_i(F)/A_*}$, $I^* = \frac{\omega A_*}{k_I}$, $R_* = \frac{\gamma_A A_* + \gamma_I I_*}{\mu}$ and $F_* = \frac{\epsilon A_*}{\xi}$. For Case I, $A_* = \frac{\mu}{\beta}\frac{R_{0H}+R_{0F}-1}{1+\frac{R_{0F}}{R_{0H}}}$ and for Case II, A_* is given by

$$(R_{0H} + 1)\mu - \beta A_* = \left(1 - \frac{\Lambda}{A_* k_A}\right)\left(1 - e^{-\frac{\alpha\epsilon A_*}{\xi}}\right)$$

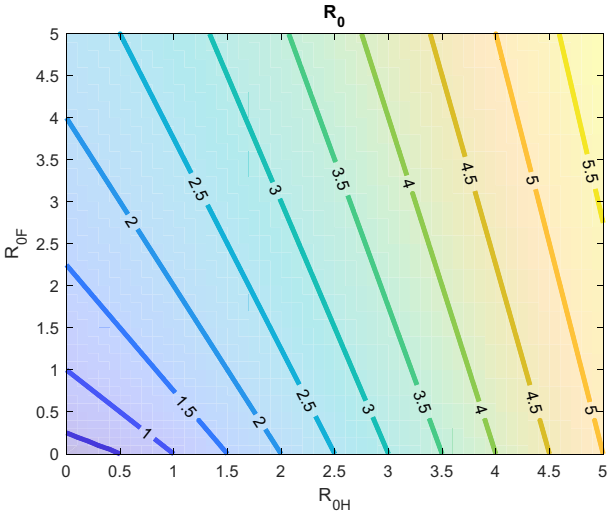

Fig. 2 Role of direct (R_0H) and indirect (R_0F) transmission in outbreak (color figure online)

It is clear that $(1 - e^{-\frac{\alpha\epsilon A_*}{\xi}}) \in [0, 1]$, otherwise the system will be unbounded below. Hence, we obtain

$$A_*^2 + \frac{1 - (R_{0H} + 1)\mu}{\beta} A_* - \frac{\Lambda}{\beta K_A} \leq 0$$

which has, at most, one positive solution for A_* as $\frac{1-(R_{0H}+1)\mu}{\beta} A_* \geq 0$ since $\mu << 1$. For Case I, the expression of A_* demonstrates that the EE exists for $R_{0H} + R_{0F} \geq 1$. However, it is cumbersome to deduce the condition for the existence of A_* in Case II. Therefore, we chose to use the center manifold theorem (Theorem 4.1 in Castillo-Chavez and Song 2004), which could help us characterize the existence and nature of the EE near $R_0 = 1$ using the Jacobian at the DFE for both the cases simultaneously.

Theorem 2 *The model exhibits forward bifurcation at* $R_0 = 1$.

Please refer to "Appendix C" for detailed proof. The above analysis nominates $R_0 = 1$ as the disease invasion threshold. The expression of R_0 clarifies the role of both direct and indirect transmissions. R_0 can be used to measure the control efforts required to mitigate or stop the spread of the disease. However, if the infection is carried by more than one types of host, the use of R_0 leads to a distinct underestimation of the requirements (Bani-Yaghoub et al. 2012; Pauline 2017). In such cases, the type reproduction number provides a significantly more accurate estimation of the required control efforts (Roberts and Heesterbeek 2003; Heesterbeek and Roberts 2007).

3.1.1 Type Reproduction Number

It is essential to gain a clear understanding of the explicit role of human carriers (direct transmission) and environmental carriers (indirect transmission) in spreading the virus so as to decide feasible and effective control strategies. The basic reproduction number properly defines the invasion threshold, but this number cannot distinguish the pathway-specific transmission. In this section, we use the concept of type reproduction number (Roberts and Heesterbeek 2003; Heesterbeek and Roberts 2007) to investigate the pathway-specific transmission. Type reproduction number for host, T_H, refers to the expected number of infectious individuals caused by one infectious individual in a completely susceptible environment, either by direct or indirect transmission. Following the notation in Roberts and Heesterbeek (2003), let I_5 be the 5×5 identity matrix, $P_H = [ph_{ij}]$ be the projection matrix defined by, $ph_{11} = 1$, and $ph_{ij} = 0$ when $i \neq 1$ or $j \neq 1$. E_H is the unit column matrix with its first element equal to 1. Then,

$$T_H = E'_H K(I_5 - (I_5 - P_H)K)^{-1} E_H = R_{0H} + R_{0F}$$

and we have the following properties (Heesterbeek and Roberts 2007).

- $T_H > 1$ iff $R_0 > 1$.
- Transmission will be terminated over time if T_H can be reduced by a factor of $v_H \geq 1 - \frac{1}{T_H}$. This reduction can be achieved by means of vaccinating susceptible individuals (as this will reduce the number of available susceptible individuals) or by quarantining infectious individuals (as this will reduce their infectious period).
- Finally, $\rho((I - P)K) = 0$, which indicates that fomites do not act as a reservoir.

Therefore, the invasion threshold can be refined in terms of the type reproduction number as $T_H = 1$. Furthermore, although the expression for R_0 is difficult to interpret from the biological point of view, the expression for T_H can be easily understood as the total number of the expected secondary infected individuals as a result of both the direct and indirect transmissions caused by one infectious individual in a completely susceptible environment. Figure 3 shows a comparison between R_0 and T_H illustrating that they both coincide at 1, but $R_0 > T_H$ below 1 and $R_0 < T_H$ above 1, which may also be confirmed by using simple algebra. Rephrasing the invasion threshold not only allows us to provide a biological interpretation but also leads us to differentiate the pathway-specific transmission strength and infer the relative requirement of the subsequent control measures (Heesterbeek and Roberts 2007). If the value of T_H is known, we can estimate the vaccination requirement. Further, if we can distinguish R_{0H} and R_{0F}, i.e., isolate pathway-specific transmission strength, we will be able to estimate required strictness in maintaining quarantine measures, and requirement of cleanliness and maintaining personal hygiene to an appropriate degree.

3.2 Stochasticity in Invasion

The expression of invasion threshold, T_H demonstrates that it is equally sensitive to R_{0H} and R_{0F}. For T_H slightly greater than 1, there might exist a nonzero probability

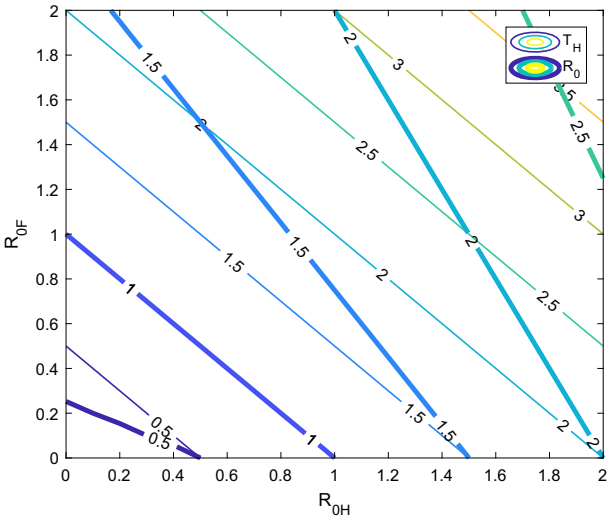

Fig. 3 Comparison of the R_0 and T_H. For the same combination of R_{0H} and R_{0F}, we compared the value of R_0 (thick lines) and T_H (thin lines) using a contour plot (color figure online)

of disease extinction. Direct transmission depends on one successful transmission from one host to another, whereas indirect transmission hinges on two successful transmissions—one from the original host to fomite and then back from fomite to another host upon survival. To inspect the potential impact of stochasticity associated with these different transmission pathways on the invasion potential, we performed a stochastic simulation using the Modified Poisson Tau-Leap algorithm (Cao et al. 2005). The technique has been explained in "Appendix D" and parameter values have also been presented. To understand the invasion potential, we simulated our model for a duration of 1 year for $T_H = R_{0H} + R_{0F} = 1.1, 1.2$, where both R_{0H} and R_{0F} vary from 0% to 100% of T_H to maintain the specified value of T_H. We ran 1000 simulations for each case. Among the 1000 simulations, the fraction of number of times infectious individuals, $A(t)$ that reaches zero provides us an approximate extinction probability, which is plotted in Fig. 4. The figure shows that when $T_H = 1.1$, $R_{0H} \leq 0.88$ and $R_{0F} \geq 0.22$, the disease goes extinct by the end of 1 year. In contrast, when $R_{0H} > 0.88$ and $R_{0F} < 0.22$, the extinction probability decreases to approximately 0.9 for both cases I ($g_1(F)$) & case II ($g_2(F)$). In contrast, when $T_H = 1.2$, $R_{0H} \leq 0.84$ and $R_{0F} \geq 0.36$, the disease goes extinct by the end of 1 year. However, when $R_{0H} > 0.84$ and $R_{0F} < 0.36$, the extinction probability decreases to approximately 0.86 for both cases I and II. Therefore, the extinction probability decreases with increasing T_H and indirect transmission has a higher chance of extinction compared to direct transmission.

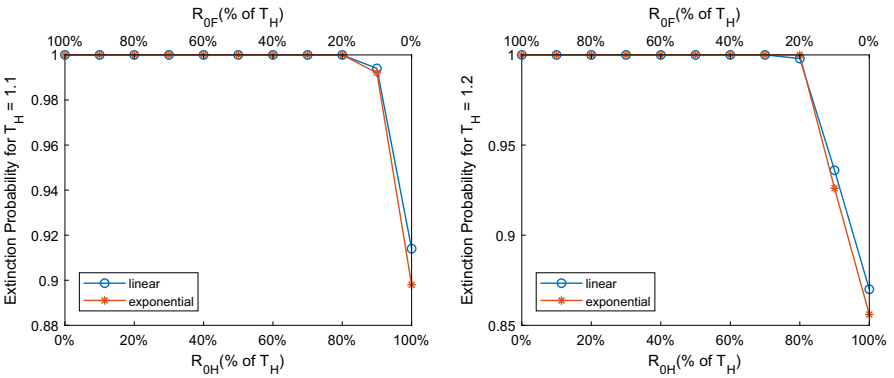

Fig. 4 Extinction probability. Approximate extinction probabilities for different combinations of R_{0H} and R_{0F} corresponding to the same T_H have been shown. The figure on the left is for $0 \geq R_{0F}, R_{0H} \geq 1.1$, whereas the figure on the right is for $0 \geq R_{0F}, R_{0H} \geq 1.2$ (color figure online)

3.3 Vaccination Threshold for Herd Immunity

In transmissible diseases, viral pathogens in existing hosts attempt to find another host to survive, proliferate and complete the cycle of transmission. At this stage, should the susceptible hosts become significantly scarce, which means that the virus is unable to find a suitable host for transmission, the transmission cycle breaks and the virus goes extinct. This is possible if the overall population has a sufficient number of immune individuals, which is defined as the state of herd immunity (Rasmussen 2020; McDermott 2021). It is a dynamic threshold that depends on the reproduction number and, consequently, on the disease transmission rate. In our present problem, this threshold is $v_c = 1 - \frac{1}{T_H}$, i.e., if v_c fraction of host becomes immune to the virus by vaccination or recovering from the infection, the pandemic will end. From the expression of v_c, it is comprehensible that if the reproduction number increases (for instance, as a consequence of increasing the transmission rate), the herd immunity threshold increases as well. Therefore, it is not rational to define a rigid threshold v_c that is less than unity, and thus remove all preventive measures.

One important information that T_H provides us with is the transmission pathway specific requirement of control measures for herd immunity. In the COVID-19 case, this allows us to distinguish between the requirements of control measures against direct transmission and those against indirect transmission. We can minimize indirect transmission in T_H by conforming to safety practices, such as general cleanliness, good hygiene, and disinfecting surfaces, while vaccination and different forms of quarantine measures can reduce the direct transmission in T_H. If we do not use any measures to prevent environmental transmission, the vaccination requirement for herd immunity, v_c, would be $v_{c,\max} = 1 - \frac{1}{R_{0H}+R_{0F}}$. Further, if we take measures for reducing the environmental transmission, the threshold (v_c) would then satisfy the inequality $1-\frac{1}{R_{0H}+R_{0F}} > v_c > 1-\frac{1}{R_{0H}}$. Provided that the environmental transmission could be completely stopped, the vaccination threshold would be reduced to $v_{c,\min} = 1 - \frac{1}{R_{0H}}$.

However, it is challenging to isolate the correct pathway specific transmission strength as fitting a model with non-identifiable set of parameters may induce errors of attributing the contribution of one transmission pathway to another. Therefore, we first check the identifiability of the parameters, which confirms the uniqueness of the estimated parameter values, and thus isolates the pathway specific transmissibility. To clarify this with examples, we fit our model with daily active cases of early epidemic data from Nigeria, Bangladesh, and USA (considering $g_1(F)$ as the fomite to human transmission function), and we then estimate the parameters β and α. The daily active cases data are taken from worldometer (https://www.worldometers.info/coronavirus/).

3.3.1 Identifiability and Fitting

Let us assume, $X = (S, A, I, R, F)$ and denote the right side of the system (1) by $\mathbb{F}$. Further, $\mathbb{P} = (\beta, \alpha)$ be the vector of parameters to be estimated. We assume the remaining parameters to be known and summarize in Table 1 with proper citation. Here, $I(t, \mathbb{P})$ is the vector of observable and $i(t, \mathbb{P})$ is the observed data at $t = 1, 2, \ldots, 40$ days. We assume $i(t, \mathbb{P})$ follow Poisson distributed with mean $I(t, \mathbb{P})$, then the maximum likelihood function will be:

$$L(i(t, \mathbb{P})) \mid I(t, \mathbb{P})) = \prod_{k=1}^{40} \frac{I(t_k)^{i(t_k)} e^{-I(t_k)}}{i(t_k)!}.$$

As ln is a monotonically increasing function, we minimize the negative log likelihood function (NLF) instead of maximizing the likelihood function for computational convenience. The NLF is reduced to:

$$\text{NLF} = -\sum_{k=1}^{40} i(t_k) \ln\left(I(t_k)\right) + \sum_{k=1}^{40} I(t_k) + \sum_{k=1}^{40} \ln(i(t_k)!).$$

As the last term in the above equation remains unchanged, it is sufficient to minimize the sum of the first two terms. Therefore, the fitting process reduces to a minimization problem as,

$$\min(\text{NLF}) = \min\left(-\sum_{k=1}^{40} i(t_k) \ln\left(I(t_k)\right) + \sum_{k=1}^{40} I(t_k)\right)$$

subject to

$$\begin{aligned} &\frac{\mathrm{d}}{\mathrm{d}t} X(t, \mathbb{P}) = \mathbb{F}(X, \mathbb{P}, t) \\ &I(0) = I_0 \\ &X(t), \mathbb{P} \geq 0 \end{aligned} \tag{3}$$

Table 1 Values of the model parameters corresponding to the COVID-19 cases in USA, Bangladesh, and Nigeria

Parameter	Value (day^{-1})	References
USA		
Λ	11, 527.9	Assuming 328.2 million population at the beginning
μ	$3.5125e{-}05$	Assuming 78 year mean life time
ω	$\frac{1}{5.2}$	Okuonghae and Omame (2020)
β	$--$	Estimated(fitting)
$\rho\pi$	$--$	Estimated(fitting)
γ_A	$\frac{1}{10}$	Adewole et al. (2021)
γ_I	$\frac{1}{14}$	Masud et al. (2020)
δ	0.03	Assumed
ϵ	2.3	Yang and Wang (2020)
ξ	1	Yang and Wang (2020)
Bangladesh		
Λ	6088.3	Assuming 160 million population at the beginning
μ	$3.8052e-05$	Assuming 72 year mean life time
ω	$\frac{1}{5.2}$	Okuonghae and Omame (2020)
β	$--$	Estimated (fitting)
$\rho\pi$	$--$	Estimated (fitting)
γ_A	$\frac{1}{10}$	Adewole et al. (2021)
γ_I	$\frac{1}{14}$	Garba et al. (2020)
δ	0.0039	Masud et al. (2020)
ϵ	3	Assumed
ξ	1	Yang and Wang (2020)
Nigeria		
Λ	10197.8	Assuming 201 million population at the beginning
μ	$5.0736e-05$	Assuming 54 year mean lifetime
ω	$\frac{1}{5.2}$	Okuonghae and Omame (2020)
β	$--$	Estimated (fitting)
$\rho\pi$	$--$	Estimated (fitting)
γ_A	$\frac{1}{10}$	Adewole et al. (2021)
γ_I	$\frac{1}{14}$	Garba et al. (2020)
δ	0.054	Garba et al. (2020)
ϵ	4	Assumed
ξ	1	Yang and Wang (2020)

The above fitting problem will provide practically feasible and unique parameters values if $\mathbb{P}$ is identifiable. The parameters $\mathbb{P}$ is structurally identifiable if a unique solution $X(t, \mathbb{P})$ exists for each $\mathbb{P}$ and a fixed initial condition. First, we estimate the fisher information matrix (FIM) and then compute the profile likelihoods to confirm the identifiability of the parameters.

We have observations at 40 distinct times, a system of 5-state variables, and two unknown parameters. Therefore, the sensitivity matrix M consists of 5 time-dependent 5×2 blocks $\mathbb{A}(t_k)$

$$M = \begin{bmatrix} \mathbb{A}(t_1) \\ \mathbb{A}(t_2) \\ \vdots \\ \mathbb{A}(t_5) \end{bmatrix}$$

where $\mathbb{A}_{jn}(t_k) = \dfrac{\partial x_j(t_k, \mathbb{P})}{\partial P_n}, \quad k = 1, \ldots, 40, \ n = 1, 2$ and $j = 1, \ldots, 5$.

The 2×2 FIM is $FIM = M^T M$, which has 2 columns. Let us denote the parameter estimates as $\hat{\beta}$ and $\hat{\alpha}$. We approximate the FIM numerically by perturbing $\hat{\beta}$ to the values $\hat{\beta^+} = (1 + 0.001)\hat{\beta}$ and $\hat{\beta^-} = (1 - 0.001)\hat{\beta}$, for which we integrate the model for each observation time. Then, we approximate the derivatives, $\mathbb{A}_{j1}(t_k) = \dfrac{\partial x_j(t_k, \hat{\beta}, \hat{\alpha})}{\partial \hat{\beta}}, \ k = 1, \ldots, 40, \ j = 1, \ldots 5$ numerically, whereas $\hat{\alpha}$ remain fixed. This provides the first column. We repeat the same process for $\hat{\alpha}$ to obtain the second column. Then, we check the rank of the matrix FIM, which is 2, which ensures that the parameters have no implicit dependency. This confirms the structural identifiability numerically. Further. we investigate practical identifiability to confirm whether the parameters estimated by fitting this model with this set of data are capable of differentiating the role of the different transmission pathways.

To investigate practical identifiability, we compute the profile likelihood of the parameters β and α. Profile likelihood reveals the dependency of the NLF on each parameter, and exposes the minimization of the NLF at the estimated value. The desired profile likelihoods are as follows:

$$PL_\beta(\beta) = \min_\alpha \left\{ NLF(\beta, \alpha) \right\} \text{ and } PL_\alpha(\alpha) = \min_\beta \left\{ NLF(\beta, \alpha) \right\}$$

where $\beta \in [\hat{\beta}(1 - 0.05), \hat{\beta}(1 + 0.05)]$ and $\alpha \in [\hat{\alpha}(1 - 0.05), \hat{\alpha}(1 + 0.05)]$.

Figure 5 shows the fitting along with the profile likelihood of the parameters which shows unique minima of the NLF at the estimated value of the parameters (second and third column) and hence confirms the identifiability which informs pathway specific transmission potential. The corresponding estimates of the reproduction numbers along with bounds for vaccination threshold are shown in Table 2 for each of the three countries.

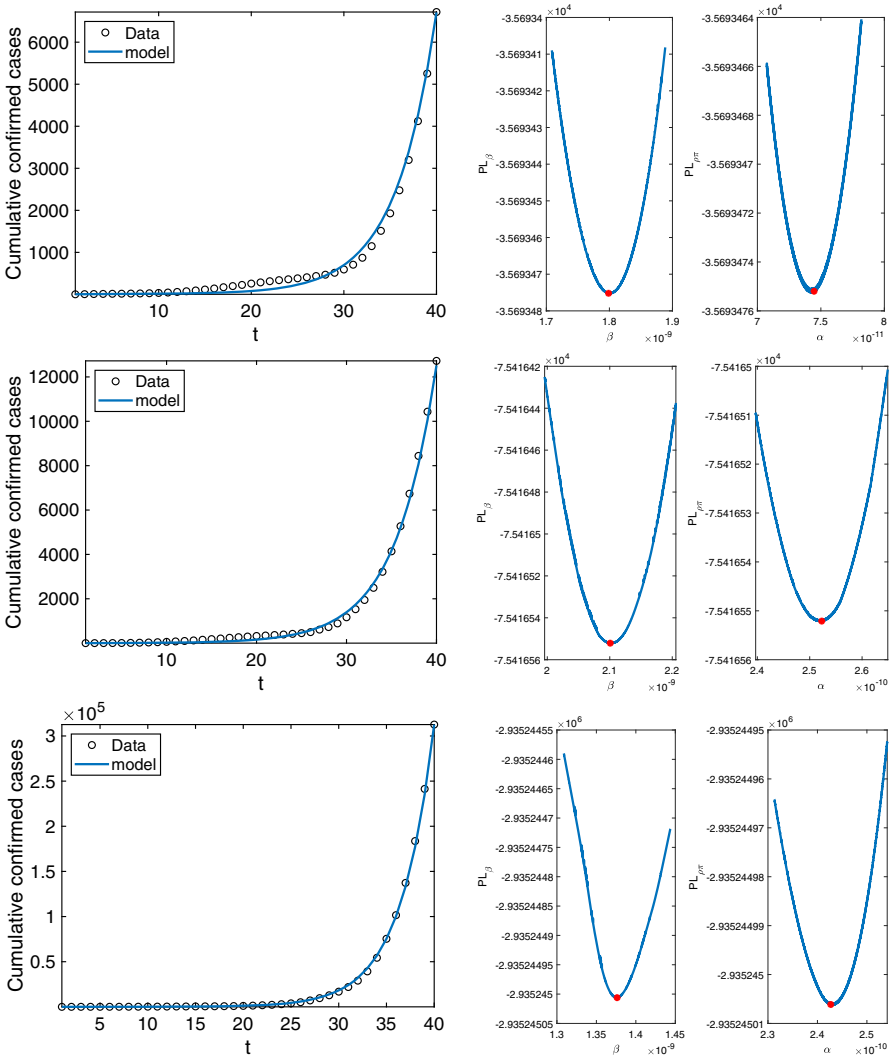

Fig. 5 Data fitting with Likelihood profile. Graphs showing data fitting and likelihood profiles of the estimated parameters for the early days of COVID-19 outbreak in Nigeria, Bangladesh, and USA, respectively (color figure online)

3.4 Role of Environmental Transmission

Figure 6 depicts the vaccination thresholds for these three different countries as a function of R_{0F}, and it clearly shows that the vaccination threshold would be decreased to a minimum value $v_{c,\min} = 1 - \frac{1}{R_{0H}}$ when $R_{0F} = 0$, i.e., the vaccination requirement would reach its minimum value $v_{c,\min}$, which is the y-intercept, if we manage to take sufficient measures to ensure no environmental/indirect transmission. In contrast, when the environmental transmission is partially halted, or if no measures are taken

Table 2 Country wise estimated rates of invasion and vaccination thresholds (approx.)

Country	R_{0H}	R_{0F}	T_H	$v_{c,\min}$	$v_{c,\max}$
Nigeria	1.24	0.20	1.44	0.191	0.306
Bangladesh	1.15	0.41	1.56	0.130	0.360
USA	1.54	0.63	2.17	0.353	0.539

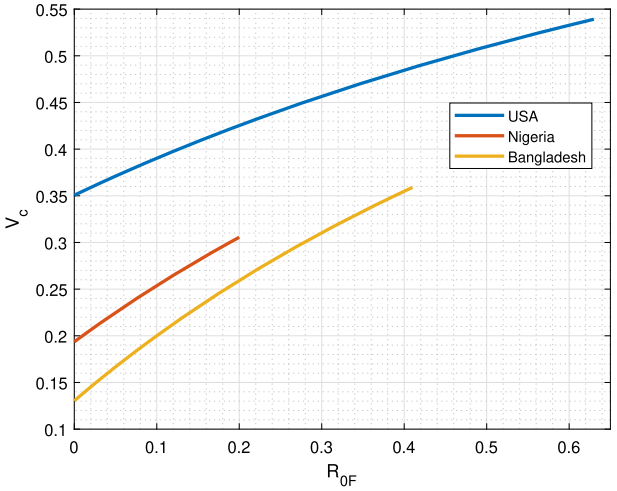

Fig. 6 Estimated vaccination threshold. Graph showing the vaccination thresholds for USA, Nigeria, and Bangladesh as a function of R_{0F}. Early COVID-19 data from Nigeria, Bangladesh, and USA were used for the estimation. Data are available online on Worldometer at https://www.worldometers.info. The estimated vaccination thresholds for these countries are 0.539, 0.306, and 0.360, respectively. However, these could be further decreased to a minimum of 0.353, 0.191, and 0.130, respectively, by reducing R_{0F}, i.e., preventing indirect transmission (color figure online)

whatsoever, the vaccination threshold would be increased to a maximum value of $v_{c,\max} = 1 - \frac{1}{R_{0H}+R_{0F}}$ depending on the size of R_{0F}. Moreover, as the indirect transmission possess higher chance of extinction than direct transmission, the additional indirect transmission would not increase the probability of invasion. According to our estimation from early epidemic data, provided that we limit indirect transmission, the vaccination threshold can be reduced to a minimum of 0.191, 0.130, and 0.353, in the cases of Nigeria, Bangladesh, and USA, respectively. Table 1 summarizes other parameter values used in the simulations for these three countries. It is noteworthy that as time will pass by, the estimate of both T_H and v_c will change.

4 Discussion and Conclusion

SARS-CoV-2 can survive on different types of surfaces and has the potential to be transmitted to susceptible individuals. Therefore, our model has considered two types of transmission routes: human-to-human (direct transmission) and human to environmental fomites and then back to human (indirect transmission). Both transmission routes contribute to the reproduction number, and the degree of this epidemic is enhanced when the sum of the contribution of both direct and indirect transmissions in the

type reproduction number exceeds one. The deterministic result shows that the invasion threshold is equally sensitive to both transmission routes. However, the stochastic simulation reveals that it is the indirect transmission that has a lower invasion potential compared to direct transmission.

Our analysis demonstrates that to develop effective control strategies, it is important to differentiate the role of these two different routes. The explicit modeling of both transmission routes and the estimation of the associated reproduction rates can allow us to gain a greater understanding of the indirect transmission epidemic potential and extent of efforts and measures that should be implemented in terms of disinfecting our proximal environment and maintaining personal hygiene. The analysis shows that the epidemic may persist even if direct transmission is reduced to 0 (for example, by social distancing and/or vaccination), whereas the reproduction number due to indirect transmission is > 1 (for example, due to lack of personal hygiene). Similarly, the epidemic may persist even if the indirect transmission is reduced to 0, whereas the reproduction number due to the direct transmission is > 1. It should be noted that it might not be practically feasible to reduce transmission from either routes to 0. If the reproduction number due to the direct transmission is < 1 but the type reproduction number is > 1, the epidemic could simply be terminated by maintaining strict cleanliness only. Moreover, the environmental transmission has lower invasion potential then the direct transmission. This nourishes the conclusion that, once the strength of the environmental transmission is known, direct transmission can be contained by using focused controls, such as the vaccination and/or different forms of quarantine.

Having obtained the sensitive quantification of the epidemic potential of the environmentally mediated transmission, mitigating environmental transmission by cleanliness, personal hygiene, and disinfection of the contaminated surfaces would reduce the requirement of human oriented control efforts. Note that individuals with either vaccine or acquired immunity may not be responsible for direct transmission but may play a plausible role in indirect transmission by acting as carrier. Besides, the herd immunity threshold is not a steady state; instead, it may increase due to the increasing transmission rate or increase in susceptible individuals due to loss of immunity. Therefore, having a fraction of individuals with immunity does not allow us to abort all preventive measures. Moreover, besides the implementation of vaccines, SARS-CoV-2 is rapidly developing mutations and it is likely that the vaccine-related antibodies may become ineffective to the new strains. We, therefore, conclude that all possible transmission routes need to be carefully considered and measured while vaccinating the population until the transmission is fully under control or declared eradicated.

Apart from fomite-mediated transmission, indirect transmission also includes transmission through aerosol particles deposited in the air by droplets, as suggested by Leung (2021), Castaño et al. (2021) and Aydogdu et al. (2021). However, aerosol mediated transmission is highly dependent on the respective air circulation and the physical structure of the venue. The deposition and decay rates can vary significantly. Furthermore, consideration of both indirect routes would lead to difficulties in terms of estimating the parameters associated with them. Despite this limitation, our study provides a clear indication that all possible transmission routes need to be carefully considered, and their transmission potential needs to be accurately quantified to mea-

sure the required accurate threshold for achieving herd immunity. Lastly, in estimating herd immunity and planning control strategies, immunity loss and the probability of reinfection should be considered as well, two issues that form the core of our future research studies.

Funding This work is supported by the National Research Foundation of Korea (NRF) Grant funded by the Korea Government (NRF-2017R1E1A1A03069992).

Data Availability Data have been taken from worldometer (https://www.worldometers.info/coronavirus/).

Declarations

Conflict of Interest All the authors declare that there is no conflict of interest.

Ethical Approval Not applicable.

Consent to Participate Not applicable.

Consent for Publication All the authors give consent.

Code Availability Available on request.

Appendix A: Next Generation Matrix

To find the basic reproduction number, we follow the next generation method (van den Driessche and Watmough 2002) and system (1) is written in the following form:

$$\dot{x} = \mathcal{F}(x) - (\mathcal{V}^{-}(x) - \mathcal{V}^{+}(x)) \tag{A1}$$

where $\mathcal{F}$, $\mathcal{V}^{-}$, and $\mathcal{V}^{+}$ are as follows:

$$\mathcal{F} = \begin{pmatrix} \beta AS + \rho S f_i(F) \\ \epsilon A \\ 0 \\ 0 \\ 0 \end{pmatrix}, \mathcal{V}^{-} = \begin{pmatrix} k_A A \\ \xi V \\ k_I I \\ \mu R \\ \beta AS + \rho S f_i(F) + \mu S \end{pmatrix},$$

$$\mathcal{V}^+ = \begin{pmatrix} 0 \\ 0 \\ \omega A \\ \gamma_A A + \gamma_I I \\ \Lambda \end{pmatrix}$$

and $x = (A, F, I, R, S) \in \mathbb{R}^+_5$. Here, the rate of appearance of new infections is represented by the elements of $\mathcal{F}$ and the rate of transfer of individuals into and out of the compartments are in $\mathcal{V}^+$ and $\mathcal{V}^-$, respectively. The Jacobian of $\mathcal{F}$ at $\mathcal{E}_0$ takes the following form.

$$Jacobian(\mathcal{F})_{\mathcal{E}_0} = \left(\begin{array}{cc|ccc} \beta\frac{\Lambda}{\mu} & \rho\frac{\Lambda}{\mu} f_i'(F) & 0 & 0 & 0 \\ \epsilon A & 0 & 0 & 0 & 0 \\ \hline 0 & 0 & 0 & 0 & 0 \\ 0 & 0 & 0 & 0 & 0 \\ 0 & 0 & 0 & 0 & 0 \end{array}\right)$$

As only the first 2×2 block of the above matrix is nonzero, whatever multiplied with it would result in a similar matrix with only a first 2×2 nonzero block. So, it suffices to consider a 2×2 matrix instead of a 5×5 matrix. Following van den Driessche and Watmough (2002), we write the sub-matrices $\mathfrak{F}$ and $\mathfrak{V}$ as

$$\mathfrak{F} = \left(\frac{\partial \mathcal{F}_i}{\partial x_j}\right)_{\mathcal{E}_0, 1 \le k, j \le 2} = \begin{pmatrix} \beta\frac{\Lambda}{\mu} & \rho\frac{\Lambda}{\mu} f_i'(F) \\ \epsilon & 0 \end{pmatrix}, \mathfrak{V} = \left(\frac{\partial \mathcal{V}_i}{\partial x_j}\right)_{\mathcal{E}_0, 1 \le i, j \le 3} = \begin{pmatrix} k_A & 0 \\ 0 & \xi \end{pmatrix}$$

Appendix B: Proof to Theorem 1

Proof Conferring the symbols from equation (A1), we verify the following at $\mathcal{E}_0$.

- If $x \ge 0$, then $\mathcal{F}_i, \mathcal{F}_i^-, \mathcal{V}_i^+ \ge 0$ for $i = 1, 2, \ldots, 5$.
- If $x_i = 0$, then $\mathcal{V}_i^- = 0$.
- $\mathcal{F}_i = 0$ if $i > 2$.
- At $\mathcal{E}_0$, $\mathcal{F}_i(x) = 0$ and $\mathcal{V}_i^+(x) = 0$.
- Finally, all eigenvalues of $\mathfrak{V}_{\mathcal{E}_0}$ are positive.

Therefore, theorem 2 from van den Driessche and Watmough (2002) completes the proof. □

Appendix C: Proof to Theorem 2

Proof For computational convenience, we assume k_A as the bifurcation parameter. At $R_0 = 1$,

$$k_A^* = \frac{\Lambda\beta}{\mu} + \frac{\Lambda\epsilon\pi\rho}{\mu\xi}$$

The largest eigenvalue of the Jacobian of the system at DFE and k_A^* is 0 with multiplicity one. In addition, there is a nonnegative left eigenvector and a nonnegative right eigenvector corresponding to the 0 eigenvalue. The local dynamics are then determined by the two constants a and b defined in Theorem 4.1 of Castillo-Chavez and Song (2004). For our model, $a = -\frac{\beta}{2}$ and $b = \frac{\xi^2\mu}{\Lambda\epsilon\pi\rho}k_A^{*2}$, which indicates that a positive EE exists and it is locally asymptotically stable for $R_0 > 1$. □

Appendix D: Modified Poisson Tau-Leap Algorithm

The model (1) can be split into the following 12 reactions:

$$\begin{aligned}
R_1 &: \xrightarrow{K_1} S\\
R_2 &: S \xrightarrow{K_2}\\
R_3 &: S \xrightarrow{K_3(DirectTransmission)} A\\
R_4 &: S \xrightarrow{K_4((IndirectTransmission))} A\\
R_5 &: A \xrightarrow{K_5}\\
R_6 &: A \xrightarrow{K_6} R\\
R_7 &: A \xrightarrow{K_7} I\\
R_8 &: I \xrightarrow{K_8}\\
R_9 &: I \xrightarrow{K_9} R\\
R_{10} &: R \xrightarrow{K_{10}}\\
R_{11} &: \xrightarrow{K_{11}} F\\
R_{12} &: F \xrightarrow{K_{12}}
\end{aligned} \tag{D2}$$

and the corresponding propensities are as follows: $a_1 = \Lambda, a_2 = \mu S(t), a_3 = \beta A(t)S(t), a_4 = S(t)g_i(F(t)), a_5 = \mu A(t), a_6 = \gamma_A A(t), a_7 = \omega A(t), a_8 = (\mu + \delta)I(t), a_9 = \gamma_I I(t), a_{10} = \mu R(t), a_{11} = \epsilon A(t)$, and $a_{12} = \xi F(t)$, respectively. The stoichiometry matrix is provided by the following matrix:

$$v = \begin{pmatrix} v_1 \\ v_2 \\ \vdots \\ v_{12} \end{pmatrix} = \begin{pmatrix} 1 & 0 & 0 & 0 & 0 \\ -1 & 0 & 0 & 0 & 0 \\ -1 & 1 & 0 & 0 & 0 \\ -1 & 1 & 0 & 0 & 0 \\ 0 & -1 & 0 & 0 & 0 \\ 0 & -1 & 0 & 1 & 0 \\ 0 & -1 & 1 & 0 & 0 \\ 0 & 0 & -1 & 0 & 0 \\ 0 & 0 & -1 & 1 & 0 \\ 0 & 0 & 0 & -1 & 0 \\ 0 & 0 & 0 & 0 & 1 \\ 0 & 0 & 0 & 0 & -1 \end{pmatrix} \tag{D3}$$

The propensity vector $a = [a_1(X), a_2(X), \ldots, a_{12}(X)]^T$ along with the state change vectors $v_1, v_2, \ldots, v_{12}$ describe the reactions $R_1, R_2, \ldots, R_{12}$,respectively.

$$\nabla a := \begin{pmatrix} \nabla a_1 \\ \nabla a_2 \\ \vdots \\ \nabla a_{12} \end{pmatrix} = \begin{pmatrix} 0 & 0 & 0 & 0 & 0 \\ \mu & 0 & 0 & 0 & 0 \\ \beta A(t) & \beta S(t) & 0 & 0 & 0 \\ g_i(F(tt)) & 0 & 0 & 0 & \frac{\partial g_i(F)t))}{\partial F} S(t) \\ 0 & \mu & 0 & 0 & 0 \\ 0 & \gamma_A & 0 & 0 & 0 \\ 0 & \omega & 0 & 0 & 0 \\ 0 & 0 & \mu + \delta & 0 & 0 \\ 0 & 0 & \gamma_I & 0 & 0 \\ 0 & 0 & 0 & \mu & 0 \\ 0 & \epsilon & 0 & 0 & 0 \\ 0 & 0 & 0 & 0 & \xi \end{pmatrix}$$

$$\psi = \nabla a * v^T * a, \sigma^2 = (\nabla a * v^T)^2 * a$$

Here, $(.)^2$ stands for the element-wise square and $*$ stands for the matrix product. Therefore, following Cao et al. (2005) we define

$$\tau := \min_{j \in \{1,2,3,\ldots,12\}} \left(\frac{\varepsilon a_0}{|\psi_j|}, \frac{\varepsilon^2 a_0^2}{\sigma_j^2} \right).$$

Algorithm 1 Modified

1: Initialize the 5 class of population and their initial numbers $S(0)$, $A(0)$, $I(0)$, $R(0)$, $F(0)$;
2: Initialize the propensity matrix a and the stoichiometric matrix v;
3: Initialize the current time $t = 0$;
4: At time t for state x, evaluate the propensity matrix a, its gradient ∇a, and $a_0 = \sum_{j=1}^{12} a_j$;
5: Find the set of indices, c_i of the currently critical reactions for which $a_j(x(t)) > 0$ and $L_j \leq n_c$;
6: Compute the largest possible time step τ' that would not allow any propensity function to change its value by more than εa_0, where the index j runs over the currently critical reactions identified in step 5. If there are no critical reactions assign $\tau' = \infty$.
7: If $\tau' < \frac{10}{a_0}$, reject it and run SSA (Gillespie 1976) and proceed to the next time step. Otherwise, continue to the next step.
8: Compute the sum of the propensity functions of the critical functions $a_0^c(x(t)) = \sum_{j \in c_i} a_j(x)$ and generate $\tau'' = \frac{1}{a_0^c(x(t))} ln(\frac{1}{r})$ where $r \sim \mathcal{U}(0, 1)$.
9: If $\tau' < \tau''$, assign $\tau \leftarrow \tau'$, for all the critical reactions R_j, set $k_j = 0$.
10: If $\tau' \geq \tau''$, assign $\tau \leftarrow \tau''$, generate j_c as a sample of the integer random variable following $j_c = \min_{j_c \in c_i} \{j_c \mid \sum_{k=1}^{j_c} a_k(x) > r_2 \sum_{k \in c_i} a_k(x)\}$. Set $k_{j_c} = 1$, and for all the other critical reactions set $k_j = 0$, where $j \in c_i$.
11: For all the noncritical reactions R_j, generate $k_j \sim Poisson(a_j(x(t))\tau)$.
12: If $\min\{x + \sum_{j=1}^{12} k_j v_j\} < 0$ assign $\tau' \leftarrow \frac{\tau'}{2}$ and return to step 9.
13: Assign $t \leftarrow t + \tau$ and $x \leftarrow x + \sum_{j=1}^{12} k_j v_j$.
14: Record (t, x) and return to step 5 until t reach the end of the time span.

Furthermore, $L_j = \min_{i\in\{1,2,\ldots,5\}}^{(v_{ij}<0)} \left[\frac{x_i}{|v_{ij}|}\right]$. Here, the square bracket represents the "greatest integer" operator. The simulation is completed according to Algorithm 1.

References

Adewole MO, Onifade AA, Abdullah FA, Kasali F, Ismail AI (2021) Modeling the dynamics of COVID-19 in Nigeria. Int J Appl Comput Math 7(3):1–25

Al-Tawfiq JA, Memish ZA (2016) Drivers of MERS-CoV transmission: what do we know? Expert Rev Respir Med 10(3):331–338

Aydogdu M, Altun E, Chung E, Ren G, Homer-Vanniasinkam S, Chen B, Edirisinghe M (2021) Surface interactions and viability of coronaviruses. J R Soc Interface 18:20200798

Azimi P, Keshavarz Z, Cedeno Laurent JG, Stephens B, Allen JG (2021) Mechanistic transmission modeling of COVID-19 on the diamond princess cruise ship demonstrates the importance of aerosol transmission. Proc Natl Acad Sci 118(8):25. https://doi.org/10.1073/pnas.2015482118

Azuma K, Yanagi U, Kagi N, Kim H, Ogata M, Hayashi M (2020) Environmental factors involved in SARS-COV-2 transmission: effect and role of indoor environmental quality in the strategy for COVID-19 infection control. Environ Health Prev Med 25:66. https://doi.org/10.1186/s12199-020-00904-2

Bai Y, Yao L, Wei T, Tian F, Jin D-Y, Chen L, Wang M (2020) Presumed asymptomatic carrier transmission of COVID-19. JAMA 323(14):1406–1407

Bani-Yaghoub M, Gautam R, Shuai Z, van den Driessche P, Ivanek R (2012) Reproduction numbers for infections with free-living pathogens growing in the environment. J Biol Dyn 6(2):923–940

Breban R, Drake JM, Stallknecht DE, Rohani P (2009) The role of environmental transmission in recurrent avian influenza epidemics. PLoS Comput Biol 5(4):1–11

Brown JC, Virtanen J, Aaltonen K, Kivistö I, Sironen T (2021) Survival of SARS-CoV-2 on clothing materials. Adv Virol. https://doi.org/10.1155/2021/6623409

Cao Y, Gillespie DT, Petzold LR (2005) Avoiding negative populations in explicit Poisson tau-leaping. J Chem Phys 123(5):054104. https://doi.org/10.1063/1.1992473

Castaño N, Cordts SC, Jalil MK, Zhang K, Koppaka S, Bick A, Paul A, Tang S (2021) Fomite transmission, physicochemical origin of virus-surface interactions, and disinfection strategies for enveloped viruses with applications to SARS-CoV-2. ACS Omega 6:6509–6527

Castillo-Chavez C, Song B (2004) Dynamical models of tuberculosis and their applications. Math Biosci Eng 1:361

Chin AWH, Chu JTS, Perera MRA, Hui KPY, Yen H-L, Chan MCW, Peiris M, Poon LLM (2020) Stability of SARS-CoV-2 in different environmental conditions. Lancet Microbe. https://doi.org/10.1016/S2666-5247(20)30003-3

Eisenberg JNS, Lei X, Hubbard AH, Brookhart MA, Colford J, John M (2005) The role of disease transmission and conferred immunity in outbreaks: analysis of the 1993 cryptosporidium outbreak in Milwaukee, Wisconsin. Am J Epidemiol 161(1):62–72. https://doi.org/10.1093/aje/kwi005

Garba SM, Lubuma JM-S, Tsanou B (2020) Modeling the transmission dynamics of the COVID-19 pandemic in South Africa. Math Biosci 328:108441

Gidari A, Sabbatini S, Bastianelli S, Pierucci S, Busti C, Bartolini D, Stabile AM, Monari C, Galli F, Rende M, Cruciani G, Francisci D (2021) SARS-CoV-2 survival on surfaces and the effect of UV-C light. Viruses. https://doi.org/10.3390/v13030408

Gillespie DT (1976) A general method for numerically simulating the stochastic time evolution of coupled chemical reactions. J Comput Phys 22(4):403–434. https://doi.org/10.1016/0021-9991(76)90041-3

Gonçalves J, da Silva PG, Reis L, Nascimento MSJ, Koritnik T, Paragi M, Mesquita JR (2021) Surface contamination with SARS-CoV-2: a systematic review. Sci Total Environ 798:149231. https://doi.org/10.1016/j.scitotenv.2021.149231

Harvey AP, Fuhrmeister ER, Cantrell ME, Pitol AK, Swarthout JM, Powers JE, Nadimpalli ML, Julian TR, Pickering AJ (2021) Longitudinal monitoring of SARS-CoV-2 RNA on high-touch surfaces in a community setting. Environ Sci Technol Lett 8(2):168–175. https://doi.org/10.1021/acs.estlett.0c00875

Heesterbeek JAP, Roberts MG (2007) The type-reproduction number t in models for infectious disease control. Math Biosci 206(1):3–10. https://doi.org/10.1016/j.mbs.2004.10.013

Hirose R, Ikegaya H, Naito Y, Watanabe N, Yoshida T, Bandou R, Daidoji T, Itoh Y, Nakaya T (2020) Survival of severe acute respiratory syndrome coronavirus 2 (SARS-CoV-2) and influenza virus on human skin: importance of hand hygiene in coronavirus disease 2019 (COVID-19). Clin Infect Dis 73(11):4329–4335. https://doi.org/10.1093/cid/ciaa1517

Hirose R, Itoh Y, Ikegaya H, Miyazaki H, Watanabe N, Yoshida T, Bandou R, Daidoji T, Nakaya T (2022) Differences in environmental stability among SARS-CoV-2 variants of concern: omicron has higher stability. bioRxiv. https://doi.org/10.1101/2022.01.18.476607

Huang S-W, Wang S-F (2021) SARS-CoV-2 entry related viral and host genetic variations: implications on COVID-19 severity, immune escape, and infectivity. Int J Mol Sci 22(6):5. https://doi.org/10.3390/ijms22063060

Kim E-J, Lee D (2020) Coronaviruses: SARS, MERS and COVID-19. Korean J Clin Lab Sci 52:297–309. https://doi.org/10.15324/kjcls.2020.52.4.297

Kim UJ, Lee SY, Lee JY, Lee A, Kim SE, Choi O-J, Lee JS, Kee S-J, Jang H-C (2020) Air and environmental contamination caused by COVID-19 patients: a multi-center study. J Korean Med Sci. https://doi.org/10.3346/jkms.2020.35.e332

Leung NHL (2021) Transmissibility and transmission of respiratory viruses. Nat Rev Microbiol 19:1–18

Li S, Eisenberg JNS, Spicknall IH, Koopman JS (2009) Dynamics and control of infections transmitted from person to person through the environment. Am J Epidemiol 170(2):257–265

Li X, Xu B, Shaman J (2019) The impact of environmental transmission and epidemiological features on the geographical translocation of highly pathogenic avian influenza virus. Int J Environ Res Public Health. https://doi.org/10.3390/ijerph16111890

Lopman B, Gastanaduy P, Park GW, Hall AJ, Parashar UD, Vinjé J (2012) Environmental transmission of norovirus gastroenteritis. Curr Opin Virol 2(1):96–102

Masud M, Islam MH, Mamun KA, Kim BN, Kim S (2020) COVID-19 transmission: Bangladesh perspective. Mathematics 8(10):1793

McDermott A (2021) Core concept: herd immunity is an important and often misunderstood public health phenomenon. Proc Natl Acad Sci. https://doi.org/10.1073/pnas.2107692118

McKinney KR, Gong YY, Lewis TG (2006) Environmental transmission of SARS at Amoy gardens. J Environ Health 68(9):26

Mizumoto K, Kagaya K, Zarebski A, Chowell G (2020) Estimating the asymptomatic proportion of coronavirus disease 2019 (COVID-19) cases on board the diamond princess cruise ship, Yokohama, Japan, 2020. Eurosurveillance 25(10):2000180

Morawska L, Tang JW, Bahnfleth W, Bluyssen PM, Boerstra A, Buonanno G, Cao J, Dancer S, Floto A, Franchimon F, Haworth C, Hogeling J, Isaxon C, Jimenez JL, Kurnitski J, Li Y, Loomans M, Marks G, Marr LC, Mazzarella L, Melikov AK, Miller S, Milton DK, Nazaroff W, Nielsen PV, Noakes C, Peccia J, Querol X, Sekhar C, Seppänen O, Tanabe S-I, Tellier R, Tham KW, Wargocki P, Wierzbicka A, Yao M (2020) How can airborne transmission of COVID-19 indoors be minimised? Environ Int 142:105832. https://doi.org/10.1016/j.envint.2020.105832

Nishiura H, Kobayashi T, Suzuki A, Jung S-M, Hayashi K, Kinoshita R, Yang Y, Yuan B, Akhmetzhanov AR, Linton NM, Miyama T (2020) Estimation of the asymptomatic ratio of novel coronavirus infections (COVID-19). Int J Infect Dis 94:154–155

Okuonghae D, Omame A (2020) Analysis of a mathematical model for COVID-19 population dynamics in Lagos, Nigeria. Chaos Solitons Fractals 139:110032

Pauline VDD (2017) Reproduction numbers of infectious disease models. Infect Dis Model 2(3):288–303

Pitol AK, Julian TR (2021) Community transmission of SARS-COV-2 by surfaces: risks and risk reduction strategies. Environ Sci Technol Lett 8(3):263–269. https://doi.org/10.1021/acs.estlett.0c00966

Pottage T, Garratt I, Onianwa O, Spencer A, Paton S, Verlander NQ, Dunning J, Bennett A (2021) A comparison of persistence of SARS-CoV-2 variants on stainless steel. J Hosp Infect 114:163–166. https://doi.org/10.1016/j.jhin.2021.05.015

Rasmussen AL (2020) Vaccination is the only acceptable path to herd immunity. Medicine 1(1):21–23. https://doi.org/10.1016/j.medj.2020.12.004

Roberts MG, Heesterbeek JAP (2003) A new method for estimating the effort required to control an infectious disease. Proc R Soc B Biol Sci 270(1522):1359–1364. https://doi.org/10.1098/rspb.2003.2339

Rohani P, Breban R, Stallknecht DE, Drake JM (2009) Environmental transmission of low pathogenicity avian influenza viruses and its implications for pathogen invasion. Proc Natl Acad Sci 106(25):10365–10369. https://doi.org/10.1073/pnas.0809026106

Rothe C, Schunk M, Sothmann P, Bretzel G, Froeschl G, Wallrauch C, Zimmer T, Thiel V, Janke C, Guggemos W, Seilmaier M, Drosten C, Vollmar P, Zwirglmaier K, Zange S, Wölfel R, Hoelscher M (2020) Transmission of 2019-nCoV infection from an asymptomatic contact in Germany. N Engl J Med 382(10):970–971

Rwezaura H, Tchoumi SY, Tchuenche JM (2021) Impact of environmental transmission and contact rates on COVID-19 dynamics: a simulation study. Inform Med Unlocked 27:100807. https://doi.org/10.1016/j.imu.2021.100807

Smither SJ, Eastaugh LS, Findlay JS, Lever MS (2020) Experimental aerosol survival of SARS-COV-2 in artificial saliva and tissue culture media at medium and high humidity. Emerg Microbes Infect 9(1):1415–1417. https://doi.org/10.1080/22221751.2020.1777906

Stutt R, Retkute R, Bradley M, Gilligan C, Colvin J (2020) A modelling framework to assess the likely effectiveness of facemasks in combination with 'lock-down' in managing the COVID-19 pandemic. Proc Math Phys Eng Sci 476

van den Driessche P, Watmough J (2002) Reproduction numbers and sub-threshold endemic equilibria for compartmental models of disease transmission. Math Biosci 180(1–2):29–48

van Doremalen N, Bushmaker T, Morris DH, Holbrook MG, Gamble A, Williamson BN, Tamin A, Harcourt JL, Thornburg NJ, Gerber SI, Lloyd-Smith JO, de Wit E, Munster VJ (2020) Aerosol and surface stability of SARS-COV-2 as compared with SARS-COV-1. N Engl J Med 382(16):1564–1567

Vardoulakis S, Sheel M, Lal A, Gray D (2020) COVID-19 environmental transmission and preventive public health measures. Aust N Z J Public Health 44(5):333–335. https://doi.org/10.1111/1753-6405.13033

Vergara-Castaneda A, Escobar-Gutiérrez A, Ruiz-Tovar K, Sotelo J, Ordonez G, Cruz-Rivera MY, Fonseca-Coronado S, Martinez-Guarneros A, Carpio-Pedroza JC, Vaughan G (2012) Epidemiology of varicella in Mexico. J Clin Virol 55(1):51–57

Wang R-H, Jin Z, Liu Q-X, van de Koppel J, Alonso D (2012) A simple stochastic model with environmental transmission explains multi-year periodicity in outbreaks of avian flu. PLoS ONE 7(2):1–9. https://doi.org/10.1371/journal.pone.0028873

Wardeh M, Baylis M, Blagrove MSC (2021) Predicting mammalian hosts in which novel coronaviruses can be generated. Nat Commun 1:2. https://doi.org/10.1038/s41467-021-21034-5

Watanabe T, Bartrand TA, Weir MH, Omura T, Haas CN (2010) Development of a dose-response model for SARS coronavirus. Risk Anal 30(7):1129–1138

Wijaya KP, Ganegoda N, Jayathunga Y, Götz T, Schäfer M, Heidrich P (2021) An epidemic model integrating direct and fomite transmission as well as household structure applied to COVID-19. J Math Ind 11

Wilson AM, Weir MH, Bloomfield SF, Scott EA, Reynolds KA (2021) Modeling COVID-19 infection risks for a single hand-to-fomite scenario and potential risk reductions offered by surface disinfection. Am J Infect Control 49(6):846–848. https://doi.org/10.1016/j.ajic.2020.11.013

worldometer. https://www.worldometers.info/coronavirus/

Wormser GP (2020) COVID-19 versus seasonal influenza 2019–2020: USA. Wien Klin Wochenschr 132:387–389

Yang CY, Wang J (2020) A mathematical model for the novel coronavirus epidemic in Wuhan, China. Math Biosci Eng 17(3):2708–2724. https://doi.org/10.3934/mbe.2020148

Yang C, Wang J (2021) Transmission rates and environmental reservoirs for COVID-19—a modeling study. J Biol Dyn 15(1):86–108. https://doi.org/10.1080/17513758.2020.1869844

Yu X, Yang R (2020) COVID-19 transmission through asymptomatic carriers is a challenge to containment. Influenza Other Respir Viruses 14(4):474–475. https://doi.org/10.1111/irv.12743

Zhao J, Eisenberg JE, Spicknall IH, Li S, Koopman JS (2012) Model analysis of fomite mediated influenza transmission. PLoS ONE 7(12):1–11. https://doi.org/10.1371/journal.pone.0051984

Zhu Z, Lian X, Su X, Wu W, Marraro GA, Zeng Y (2020) From SARS and MERS to COVID-19: a brief summary and comparison of severe acute respiratory infections caused by three highly pathogenic human coronaviruses. Respir Res 2:1. https://doi.org/10.1186/s12931-020-01479-w